ACS APPLIED MATERIALS & INTERFACES

Research Article

www.acsami.org

Ligand Exchange Procedure for Bimetallic Magnetic Iron−Nickel Nanocrystals toward Biocompatible Activities

Xiang Mao,[†] Junyoung Kwon,[†] Eun Kyoung Koh,[‡] Dae Youn Hwang,*[,‡] and Jaebeom Lee*[,†]

[†]Department of Cogno-Mechatronics Engineering, Pusan National University, Busan 609-735, Republic of Korea

[‡]Department of Biomaterials Science, College of Natural Resources and Life Science, Pusan National University, 50 Cheonghak, Miryang 627-706, Republic of Korea

Supporting Information

ABSTRACT: Bimetallic magnetic iron-nickel (FeNi) nanocrystals (NCs) were synthesized through a one-pot synthetic wet chemistry method, and the morphology of the resulting NCs can be adjusted by changing the molar ratio of chemical attendees during the experimental processes. The obtained FeNi NCs can be redispersed in water medium though the phase works by using the ligand exchange procedures of cysteine (Cys), 5-aminovaleric acid (5AA), and glutathione (GSH), respectively. The synthesized NCs exhibited excellent magnetic properties with H_c (magnetic fields, $\approx 10^{-3}$ T) and μ_a (initial permeability of up to 10^5). Furthermore, linear sweep voltammetry (LSV) polarization curves revealed a low overpotential of −0.47, −0.44, and 0.15 V and a current of 105.7, 97.8, and 209 mA for the Cys-, 5AA-, and GSH-FeNi NCs, respectively. This indicated a relatively high catalytic activity of these NCs in the hydrogen evolution reaction (HER). The different cell lines (AGS, HepG2, MG63, NCI-H460, and SK-MEL-2) exposed to FeNi NCs for 5 days exhibited >87% viability at concentrations of up to 50 μg mL^{-1}, which was indicative of excellent biocompatibility. The resulting FeNi NCs offer a facile synthetic route to fabricate monodispersed NCs. The biocompatibility of these NCs should also enable their application in electrocatalysis and biological applications.

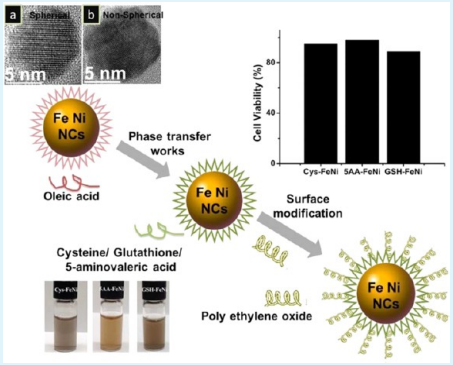

KEYWORDS: *bimetallic, iron−-nickel (FeNi) nanocrystals (NCs), magnetic, ligand exchange, biocompatibility*

1. INTRODUCTION

High sensitivity and enhanced precision diagnostics have significant potential for improving the therapeutic efficiencies of early diagnosis.[1] In particular, magnetic resonance imaging (MRI) is one of the most promising and excellent diagnostic technologies owing to the high temporal and spatial resolution of magnetic composites.[2] Therefore, multifunctional composites consisting of magnetic transition metals (Fe, Ni, Co) have attracted considerable interest owing to their potential use in applications such as MRI, catalytic measurements, and electromagnetic devices (e.g., inductors, ac−dc converters).[3] Current research is especially focused on MRI for high-frequency electromagnetic device applications,[4] and soft magnetic materials with high saturation magnetization (M_s), high permeability (μ), and low energy losses are being investigated in this regard.[5] Moreover, FeX (X = Ni, Co) alloys are considered common soft magnetic alloys, with large saturation magnetization, which can be used as ferromagnetic substitutes. These alloys are also biocompatible, owing to surface modification, and are considered a suitable contrast agent for biological applications. On the other hand, the use of these alloys in conventional high-frequency applications stems from their large permeability and low power loss;[6] they also have excellent catalytic properties owing to their nickel content. Currently, the nickel-based integrated materials are fabricated with relative ease by using conventional approaches such as Ni@Al_2O_3,[7] $NiPt_3$,[8] and NiO_X[9] nanocrystals (NCs). In these studies, nickel was used as a serviceable element for preparing multifunctional materials owing to its natural magnetic transition and possible catalytic properties. In the electrical or physical chemistry approaches, ferromagnetic materials can be considered possible multifunctional materials. In fact, the ferromagnetic materials exhibit high initial permeability even under a low magnetic field, which leads to increasing permeability with increasing saturation magnetization.[10,11] Furthermore, the excellent catalytic and magnetic properties of the nickel composites stem from their nickel components.[12,13] Developing biocompatible FeNi NCs for new magnetic substitutes in applications is therefore essential.

However, synthesis of monodispersed FeNi NCs remains quite challenging, although FeNi NCs with the desired size and shape have been obtained.[14−16] G. Viau et al.[17] prepared spherical FeNi NCs that are a few hundred nanometers large, via a nucleation and growth process in polyols solvent. Furthermore, Moghim et al.[14,15] obtained FeNi nanocubes and nanocages through a surfactant-free electrochemical method, by manipulating the growth kinetics of a bimetallic system. However,

Received: May 7, 2015
Accepted: June 26, 2015
Published: June 26, 2015

DOI: 10.1021/acsami.5b03952
ACS Appl. Mater. Interfaces 2015, 7, 15522−15530

preparing NCs via synthetic approaches is complex and typically results in uncontrollable size or morphology of the NCs. In particular, long-term chemical stability and biocompatibility in biological applications were not achieved since the modification of the NC resulted in amphiphilic ligand encapsulation;[18−20] this encapsulation led to low exchange efficiency, owing to inefficient interaction between the NC and the small molecules, and further modification led to significantly reduced exchange ratios.[21−24] In addition, hydrophilic surface modification of natural molecules such as amino acids and peptides has scarcely been studied. Amino acids and peptides are significantly better biocompatible substitutes than other molecules such as 3,4-dihydroxyhydrocinnamic acid (DHCA),[25] poly(acrylic acid), and poly(allylamine).[26] Therefore, it is necessary to find the facile synthesis of FeNi NCs and the efficient procedure for constructing the biocompatible substitutes, which includes a convenient surface modification mechanism.

To address these obstacles, we present an efficient strategy to prepare FeNi NCs with a mean diameter of less than 20 nm in a low polarity solvent, in which the obtained NCs exhibited high magnetization with negligible hysteresis and coercivity value. The surface of the NCs can be modified with biocompatible hydrophilic biomolecules such as cysteine (Cys), 5-aminovaleric acid (5AA), and glutathione (GSH). Owing to the excellent hydrophilic property and functionality of the exchanged biomolecules, the surface modification of the NCs can be easily formatted in aqueous solutions at room temperature (RT); different from other works, there is no use of amphiphilic molecules or additional heating conditions for formatting the hydrophilic monolayer. After modification with hydrophilic molecules through ligand exchange procedures, the resulting FeNi NCs exhibit high solubility in water media and physiological solutions. These NCs are apparently nontoxic *in vitro* to a series of cell lines, as confirmed by the results of an *in vitro* toxicology evaluation that revealed negligible toxicity of the modified NCs up to concentrations of 50 μg/mL. This indicates the significant potential of biocompatible FeNi NCs for use as a new type of magnetic contrast agent.

2. EXPERIMENTAL SECTION

2.1. Materials. Iron(III) acetylacetonate ($Fe(acac)_3$), nickel(II) acetylacetonate ($Ni(acac)_2$), *N*,*N*-dimethylformamide (DMF 98%), 1,2-dihydroxy dodecane (95%), oleylamine (OLA, 98%), n-octadecylamine, oleic acid, toluene (98%), diphenyl ether (DE), polyethylene glycol (PEG, M_w 15 000, 95%), 5-aminovaleric acid (5AA, 98%), cysteine (Cys, 98%), and glutathione (GSH, 98%) were purchased from Sigma-Aldrich. All the reagents and solvents obtained from commercial suppliers were used without further purification. In addition, cells such as the adenocarcinoma cell (AGS, human stomach cell), hepatoblastoma cell (HepG2, human liver cell), osteosarcoma cell (MG63, human bone cell), carcinoma cell (NCI-H460, human lung cell), and melanoma cell (SK-MEL-2, human skin cell), as well as a tumor cell line, were all obtained from the American Type Culture Collection (Rockville, MD). All cells were maintained in a humidified incubator at 37 °C under 5% CO_2 atmosphere. Penicillin and streptomycin for cell cultures were purchased from Hyclone Laboratories Inc. (Logan, UT). NaH_2PO_4 with citric acid (pH = 2.3−8.0) and NaH_2PO_4 with sodium hydroxide (pH = 8.9−12) were used as buffer solutions.

2.2. Synthesis of the Bimetallic FeNi NCs. FeNi NCs capped with oleic acid were prepared via the coprecipitation method. $Fe(acac)_3$ (0.75 mmol, 0.265 g) and $Ni(acac)_2$ (0.5 mmol, 0.129 g) were weighed out and transferred to a reaction flask; 1,2-dihydroxy dodecane, (1.5 mmol, 0.303 g), n-octadecylamine (5 mmol, 1.64 g), and oleic acid (5 mmol, 2.1 mL) were added to the reaction mixture containing 25 mL of DE (diphenyl ether) solvent. Using a 99% N_2 gas, the resulting mixture was degassed for 20 min at room temperature. The mixture was then heated to 100 °C, held at temperature for 10 min, heated to 260 °C, refluxed for 120 min, and subsequently cooled to room temperature by removing the heat source. Thereafter, the product of the reaction was handled in air. The product was collected and precipitated using absolute isopropanol (40 mL), washed three times using a mixture of toluene and methyl alcohol, and subsequently dispersed in toluene. The reactions were all performed under a flow (1000 mL/min) of 99% N_2 gas, using the standard Schlenk line technique.

2.3. Preparation of Water-Soluble FeNi NCs (Modified by Using Biocompatible Molecular Cys, 5AA, and GSH). The oleic-acid-modified NCs were repeatedly washed with a mixture of hexane and ethanol (volume ratio 1:1) in order to remove the excess chemical from their surface. The NCs were then dried under vacuum and added to a 41 mL aqueous solution containing 0.1 M L-GSH. After a 10 min ultrasonic treatment, the NCs dissolved completely and formed a light black-brown solution. The 5AA- and L-Cys-modified NCs were prepared in the same manner. Prior to mixing the ligand water solution with the dried NCs, the pH value of each solution was adjusted to approximate values of 11.00 (L-GSH), 11.30, and 10.00 for the L-GSH-, L-Cys-, and 5AA-modified NCs, respectively. An ∼1 h ultrasonic treatment resulted in well-dispersed colloidal solutions.

2.4. Fluorescence-Activated Cell Sorting (FACS) Analysis of Different Human Cells Attached to NCs (Cys-, 5AA-, and GSH-FeNi NCs). The NCs were stained with fluorescein diacetate (FDA, F7378, Sigma-Aldrich, St. Louis, MO) in order to determine the adhesion ability of living cells. FDA (3′,6′-diacetyl-flurescein), as a nonfluorescent, white hydrophobic substance, is hydrolyzed in the cytoplasm through the cell membrane, by the cytoplasmic lipase stemming from metabolic responses, and it exhibits green fluorescence (Stubberfield and Shaw, 1990). After discarding the medium, the cells were washed twice with phosphate bufere saline (PBS), and the treated FDA stock solution (5 mg FDA/1 mL acetone) was diluted with PBS (1:100) and incubated for 15 min at 37 °C. A fluorescence microscope (Eclipse TS100, Nikon, Japan) was used to examine the morphology of the cells at an excitation wavelength of 488 nm. These cells were exposed to deionized water (control) and various concentrations of modified FeNi magnetic NCs (0, 25, and 50 μg/mL) for 1, 3, and 5 days. The cells were harvested using trypsinization and 100 μL of cell suspensions for 20 min using MuseTM Annexin-V and dead cell reagent, in the dark. The Annexin-V/7-AAD positive cells were then examined with a MuseTM Cell Analyzer (MerckMillipore, Germany). Annexin-V stained cells were marked for early apoptotic only, and those double-stained with Annexin-V and 7-ADD were marked for late apoptotic.

2.5. Cell Culture and Cell Viability Assay. The HepG2 human hepatoblastoma, MG-63 human osteosarcoma, SK-MEL-2 human melanoma, AGS human gastric adenocarcinoma, and NCI-H460 human lung carcinoma cell lines were all obtained from the Korean Cell Line Bank (Seoul, Korea). The HepG2, MG-63, and SK-MEL-2 cell lines were maintained for 24−36 h in Eagle's Minimum Essential Medium (MEM, Hyclone, Logan, UT) containing 10% fetal bovine serum (FBS, Hyclone), 100 IU/mL of penicillin, and 100 μg/mL of streptomycin. The AGS cell line and NCI-H460 cell lines were cultured in RPMI 1640 (Hyclone) supplemented with 10% FBS (Hyclone), 100 IU/mL of penicillin, and 100 μg/mL of streptomycin. All cells were maintained in a humidified incubator at 37 °C under 5% CO_2 atmosphere. Cell viability and apoptosis were measured via a Muse Cell Analyzer (PB4455ENEU, Millipore Co., Billerica, MA). The cells were stained in accordance with the manufacturer-recommended method and were measured using fluorescence signal analysis equipment. The prepared cells were suspended to final cell concentrations of 1×10^5 cells/mL in the medium. For the cell viability analysis, 20 μL of suspended cells were stained with 380 μL of Muse Count and Viability Reagent (MCH100102, Millipore Co.) and incubated for 5 min at room temperature; each cell was subsequently analyzed. For apoptosis and necrosis analysis, 100 μL of suspended cells were stained with 100 μL of Muse Annexin V and Dead Cell Reagent (MCH100105, Millipore Co.) and incubated for 20 min at room temperature; each cell was then analyzed. After confluence of the cells was achieved, the cells were exposed to various concentrations (0, 25,

DOI: 10.1021/acsami.5b03952
ACS Appl. Mater. Interfaces 2015, 7, 15522−15530

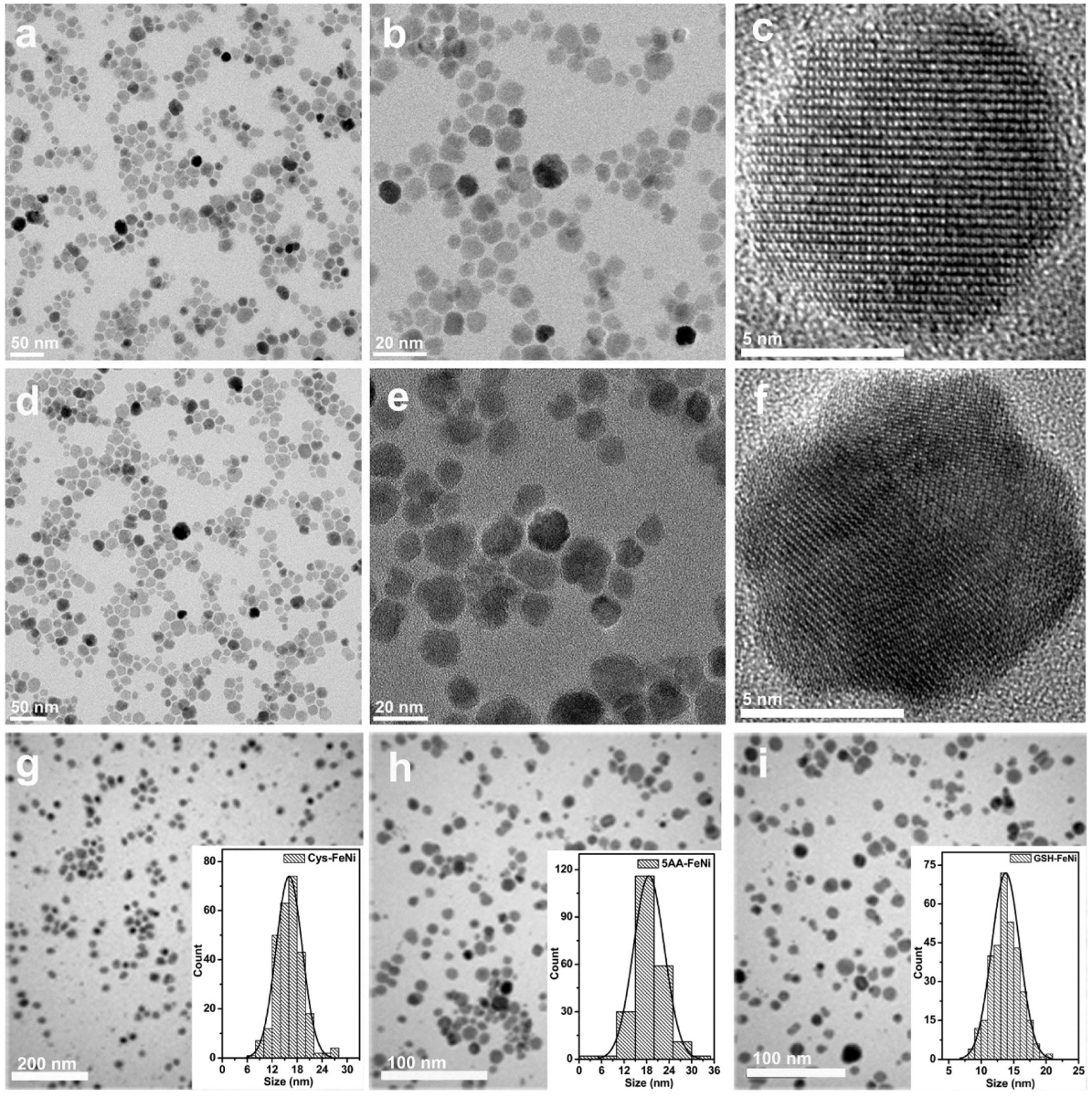

Figure 1. (a–f) Before the ligand exchange procedures, representative TEM images show the resulting FeNi NCs with sphere (a–c) and nonsphere shaped NCs during the heat-up synthesis procedure. After the ligand exchange procedures, the typical TEM images are shown for (g) Cys-FeN (16.24 ± 2.4 nm, based on 300 counts), (h) 5AA-FeNi (17.14 ± 3.1 nm, based on 214 counts), and (i) GSH-FeNi (14.54 ± 2.7 nm, based on 288 counts), respectively. Inset image shows the size distribution of each sample.

and 50 μg/mL) of Cys-, 5AA-, and GSH-modified FeNi NCs for 1, 3, and 5 days. In order to evaluate the dose-dependent effects, varying concentrations (0, 25, 50 μg/mL) of an aqueous solution of Cys-FeNi, 5AA-FeNi, and GSH-FeNi were applied for various growth periods (days) to each cell line.

2.6. Characterization. Transmission electron microscopy (TEM) and high-resolution (HR) TEM imaging were performed using a Hitachi-7600 (Japan) electron microscope to which a CCD camera (1350 × 1040) is attached; an accelerating voltage of 200 kV was used for imaging. Moreover, XRD analysis was carried out using an X-ray diffractometer (Empyrean series-2, Cu Kα radiation.). Ultraviolet (UV)–visible (vis) absorption and Fourier transform infrared (FT-IR) spectra were obtained using a Scinco S310 (Korea) and a JASCO, FT-IR 6300, respectively. The zeta potential of the samples was determined by using a 90 Plus Nanoparticle Size Analyzer (Zetasizer nano-ZS, Malvern Instruments Ltd.) in the 90° backscattering mode. Furthermore, the weight stability at high temperature was examined via thermogravimetric analysis (TGA N-1000, Korea) by heating the NCs at a rate of 15 °C per min under a nitrogen atmosphere. The corresponding magnetic properties were determined with a SQUID (superconducting quantum interference device, America) at 300 and 5 K in a field of up to 3 T, for sensitivity, field range, and temperatures of 10^{-8} emu, −7 to +7 T, and 1.7–400 K, respectively. Each sample was adjusted to a concentration of 0.05% (wt/v) in 0.01 M NaCl solution. Flow cytometry was performed on a BD FACsCalibur flow cytometer (BD Biosciences, Franklin Lakes, NJ). Linear sweep voltammetry was conducted by using an Iviumstat Electrochemical Interface (three reference electrodes method, Netherlands).

3. RESULTS AND DISCUSSION

3.1. Preparation of Bimetallic Magnetic FeNi NCs and Phase Transfer Works for Surface Modification Processes. Colloidal iron–nickel (FeNi) NCs were synthesized by dissolving an appropriate metal precursor mixture reagent (Fe^{3+}, Ni^{2+}) and oleic acid (OA) stabilizer in organic solvent and then heating this solution using carefully controlled temperature

DOI: 10.1021/acsami.5b03952
ACS Appl. Mater. Interfaces 2015, 7, 15522–15530

Scheme 1. Illustration of the Procedure Giving Rise to Biocompatible FeNi Nanoparticles by Surfactant Exchange Using Hydrophilic Molecules (Cysteine, 5-Aminovaleric Acid, and Glutathione) and Polyethylene Oxide

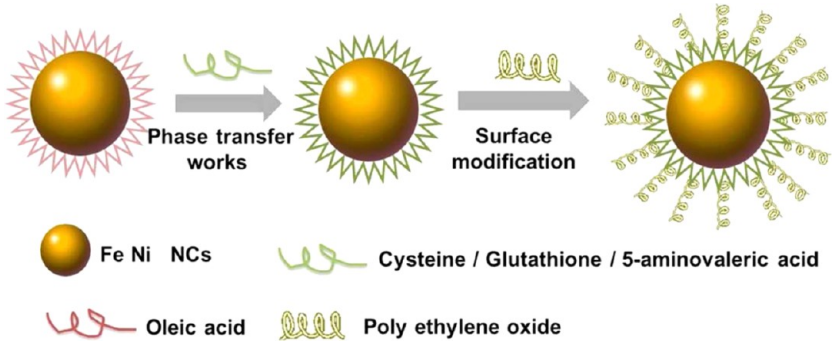

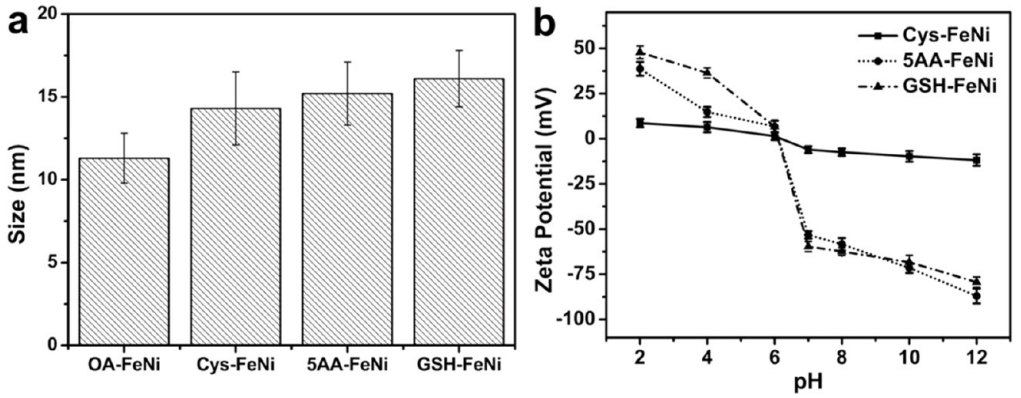

Figure 2. (a) Dynamic light scattering (DLS) size distribution of OA-FeNi, Cys-FeNi, 5AA-FeNi, and GSH-FeNi. (b) Zeta potential analysis of the pH-dependence of FeNi NCs after modification with Cys, 5AA, and GSH, respectively.

programs. The obtained FeNi NCs showed the slight difference in formatting NCs during the growth processes. The morphology was analyzed by transmission electron microcopy (TEM, Figure 1), and the size is nearly about ~10.3 ± 0.6 nm. The resulting morphology of FeNi NCs can be influenced by changing the molar ratio of metal precursors and surfactants. The nonspherical NCs were fabricated through decreasing the amount of OA in synthesis work, indicating the influences in the organic complex process. With control of the well dispersion of colloidal solution during the ligand exchange process, the quantity of NCs can be relatively decreased and can ensure the whole ligand function acted completely. The insets show the size distribution and mean diameter of the FeNi NCs after the ligand exchange by using Cys, 5AA, and GSH (Figure 1g–i). Furthermore, the strong scattering power and small lattice parameter of the FeNi structure enabled high-resolution TEM (HRTEM) analysis of the internal structure of a single NC (Figure 1c,f). This analysis revealed the formation of an ordered structure, which indicated that highly crystalline FeNi was successfully synthesized. Elemental mapping was used to further investigate spherical and nonspherical FeNi NCs, respectively. Supporting Information Figures S1 and S2 show the high angle annular dark field (HAADF)-STEM image of several representative FeNi NCs and the corresponding mapping of Fe and Ni compositions. Supporting Information Figure S3 shows the HR-TEM images of Cys-FeNi, 5AA-FeNi, and GSH-FeNi NCs, respectively. Despite the limited sensitivity of the mapping technique, the elemental analysis distribution within each nanoparticle indicates that the iron–nickel alloyed structure is formed completely as reflected in crystalline material. The X-ray diffraction (XRD) pattern of the FeNi NCs is shown in Supporting Information Figure S4. FeNi NCs, which have a diameter of 10.3 nm, exhibit two representative diffraction peaks, corresponding to the (111) and (200) planes. Moreover, the narrow size distribution during the phase change is attributed to the homogeneous distribution and lack of negative effect on the inorganic nanomaterials during the substitution of the surfactants attached to the particle surface.

Cys-, 5AA-, and GSH-capped FeNi NCs are prepared, as shown in Scheme 1. The high surface packing density of the water-soluble surfactant has a significant effect on the attainment of effective antibiofouling surfaces.[27] To achieve high molecular graft density, many anchor sites are required for functional branches. In our studies, Cys, 5AA, and GSH are used as the exchange ligands owing to their robust collective coordination to the surface of the FeNi NCs through chemical bonding linkage. The modified nanoparticle can also be completely dispersed in aqueous media. The pH of the colloidal solutions was controlled in order to ensure sufficient chemical bonding linkage between the NC surface and the functional groups of the molecules. The linkage efficiency was improved by redispersing the predried FeNi nanopowders in the solvent consisting of the completely dispersed surfactant. These NCs were then covered by polyethylene glycol (PEG), which enhanced the stability of the nanocompounds.[28,29] The resulting colloidal NCs were subsequently transferred from water to *N*,*N*-dimethylformamide (DMF), and then removed from the water under vacuum and dissolved in the DMF. Functionalized colloidal NCs were, finally, obtained after removing the unconjugated functional groups of hydrophilic molecules through further purification. After the

DOI: 10.1021/acsami.5b03952
ACS Appl. Mater. Interfaces 2015, 7, 15522–15530

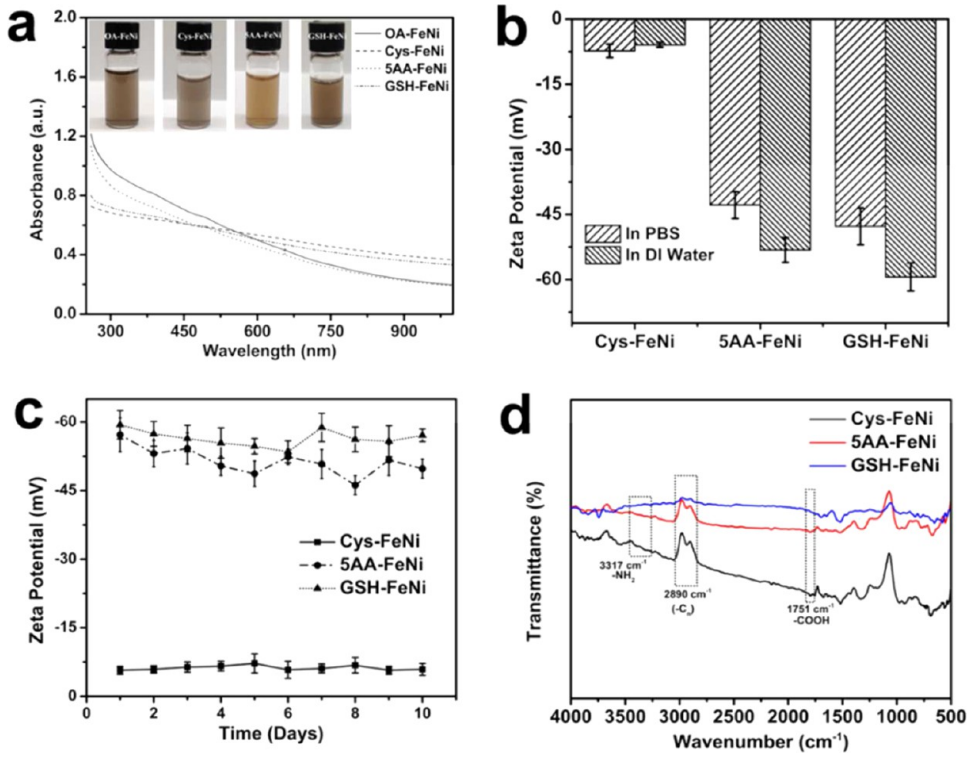

Figure 3. (a) UV−vis absorption spectra of colloidal solutions of the FeNi NCs before and after the phase transfer. Inserted digital photographs show the OA-, Cys-, 5AA-, and GSH-capped FeNi NCs (from left to right). (b) Zeta potential of the NCs (Cys-, 5AA-, and GSH-FeNi) incubated in DI water and PBS (buffer solution, pH = 7.4, 0.1 M), respectively. (c) Time-dependent zeta potential curves of Cys-, 5AA-, and GSH-FeNi, which were incubated in water. (d) FT-IR spectra of Cys-, 5AA-, and GSH-FeNi NCs for wavenumbers 500−4000 cm^{-1}. The marked peaks correspond to the primary amine group (3317 cm^{-1}), main carbon chain (2890 cm^{-1}), and carboxylic group (1751 cm^{-1}).

phase transfer, the Cys-FeNi, 5AA-FeNi, and GSH-FeNi NCs have average sizes of 16.24 ± 2.4 nm (based on 300 counts), 17.14 ± 3.1 nm (based on 214 counts), and 14.54 ± 2.7 nm (based on 288 counts), respectively. These sizes correspond closely to the TEM results; i.e., after linking with different molecules in water, the bell curve representing the diameter distribution of NCs indicates that successful phase transfer occurred, without agglomeration. The increased diameter of the NCs after the attachment of various functional groups resulted possibly from the formation of ligand layers; i.e., the size difference can be attributed to the surfactant layers attached to the particle surface. Furthermore, hydrodynamic diameters of 14.3 ± 2.2 nm (Cys-FeNi), 15.2 ± 1.9 nm (5AA-FeNi), and 16.1 ± 1.8 nm (GSH-FeNi) were determined via dynamic light scattering (DLS) analysis of the NCs in an aqueous medium (Figure 2a). The resulting FeNi NCs show the mean diameter about 11.4 ± 1.4 nm (OA-FeNi) once dispersed in organic solvent (toluene). It shows the slight increase from the diameter information and which can be ascribed to the factor of light scattering. The surface charge properties of Cys-, 5AA-, and GSH-FeNi were evaluated by measuring the zeta potentials as a function of the pH value (Figure 2b). As the figure shows, the NCs (Cys-, 5AA, or GSH-FeNi) exhibit both negative (pH = 7−12) and positive (pH = 3−7) values. The difference in the zeta potential of the NCs can be attributed to the gradual ionization of the carboxylic groups (or amino group) on their surface. In addition, the surface modification of the NCs shows that the electrokinetic behavior depends on the surface charge stemming from the adsorption of surface-active agents;[30] this surface charge developed between the surfactants and NCs in various pH media. Under various pH conditions, the water dipoles may orient at the interface between the NCs and the functional group, thereby creating a potential difference of ions or excess electrons in one or both phases. This potential difference results in a nonuniform distribution of electric charges between the different phases.[31,32] Therefore, the development of surface charge during surface modification can be attributed to the adsorption of ions after the solvent dissociates. The ionization of functional groups during surface modification also contributes to the surface charge.[33] These have a neutral surface potential in physiological environments which would lead to a longer term body fluid circulation, owing to their weak electrostatic interaction with proteins, compared to the charged NCs.[34] Moreover, the ligand exchange can be established via hydrophilic groups.

3.2. Characterization of UV−Vis Absorption, FT-IR, TGA, SQUID, and Catalytic Properties. Owing to the colloidal solution being well-dispersed at room temperature (RT), the UV absorption spectra reflect the NCs' dispersed status in Figure 3a; the inset digital image shows that NCs are well-dispersed in the water media without aggregated precipitation. In addition, the stability of the modified NCs is monitored by measuring the zeta potential in DI water and PBS solution, respectively. Values of zeta potential show the approximate equivalence which indicates that NCs keep high stability even in different solvent and after long cultivation time (Figure 3b,c). As it appeared from the above details, this stability can be ascribed to effective phase-transfer work and surface polymerization by using PEG for enhancing hydrophilic property. The covalent linkages with different ligand-modified NCs were confirmed via Fourier transform infrared (FT-IR) spectroscopy (Figure 3d). The absence of distinct IR peaks corresponding to the −SH group (2520 cm^{-1}) indicated that the

DOI: 10.1021/acsami.5b03952
ACS Appl. Mater. Interfaces 2015, 7, 15522−15530

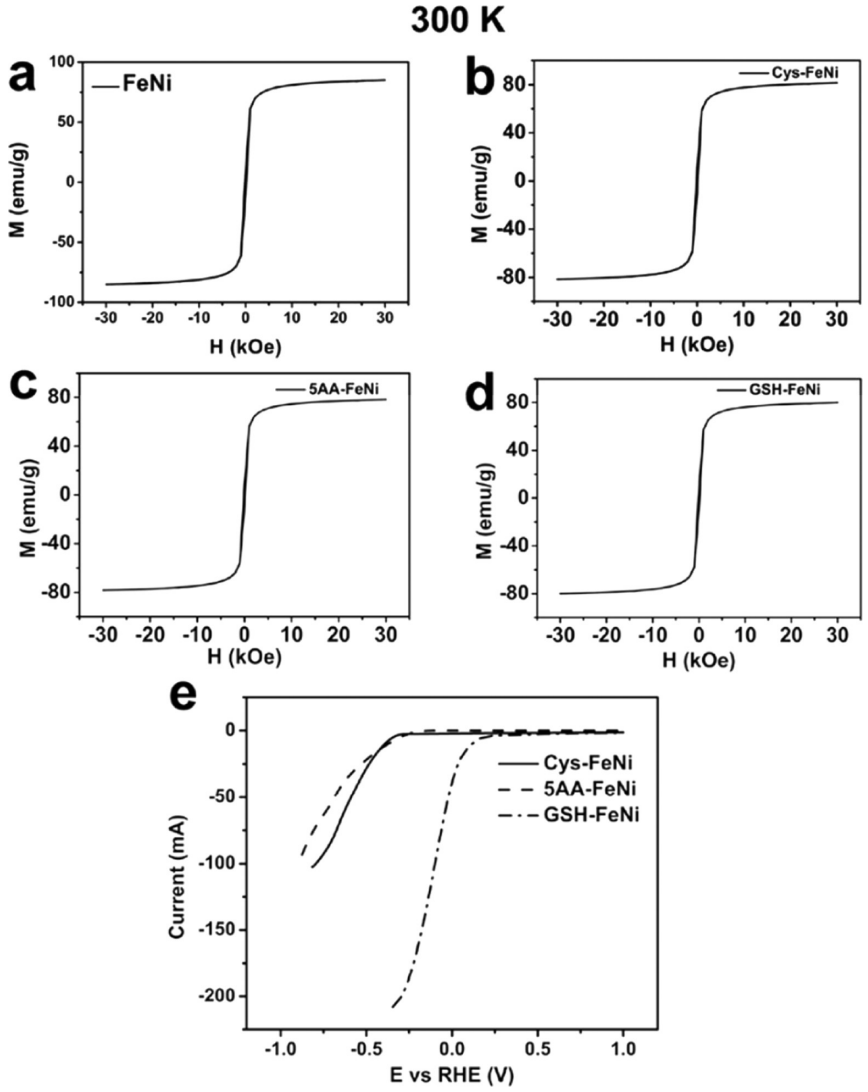

Figure 4. Magnetization (M) as a function of field (H) for FeNi NCs modified by different molecules: (a) OA-FeNi, (b) Cys-FeNi, (c) 5AA-FeNi, and (d) GSH-FeNi at 300 K. (e) Linear sweep voltammetry (LSV) polarization curves of Cys-, 5AA-, and GSH-FeNi NCs in nitrogen-purged 2 M KOH solution. Scan rate: 2 mV s^{-1}.

NCs were strongly linked to Cys and GSH, respectively, during the phase transfer. Carboxylic and amino groups are present on the surface of the FeNi NCs. However, the −SH vibration is absent from the spectra, and hence from the surface of the Cys- and GSH-capped FeNi NCs. This absence stems possibly from the covalent bonding of thiol to the NC surface.[35] Under alkaline conditions, 5AA stabilized the NC surface through linkage with carboxylic groups via electrostatic interaction in the form of electrical adsorption on the NC surface. Moreover, the low intensity of the IR peaks corresponding to the NH_2 groups (3317 cm^{-1}) results from the covalent bonding of the NH_2 group to the surface of each NC. The absorption band at 2890 cm^{-1}, which appears in all the spectra, is attributed to the stretching vibration mode of the main carbon chains of the surfactant. In addition, the functional groups of each biocompatible molecule were detected in the spectra (Supporting Information Figure S5); i.e., IR absorption bands of −COOH, $-NH_2$, and −SH were observed at 1751, 3317, and 2520 cm^{-1}, respectively. Therefore, FT-IR characterization confirmed that the hydrophilic function groups were successfully linked to the FeNi NCs. Thermogravimetric analysis (TGA) of the modified FeNi NCs (Cys-, 5AA-, GSH-NCs) was performed by heating the NCs from RT to 800 °C at a heating rate of 15 °C min^{-1}. The weight percentage of organic moieties on Cys-FeNi, 5AA-FeNi, and GSH-FeNi are ∼13.5%, 11.5%, and 15.3%, respectively. As Supporting Information Figure S6 shows, the Cys-FeNi NCs experience major (11.7%) mass loss at temperatures of 275−400 °C, which is attributed to the pyrolysis of Cys and the residual oleic acid ligands on the surface. Similarly, the 5AA-FeNi and GSH-FeNi exhibited significant mass losses of 9.7% (288−400 °C) and 14.7% (307−396 °C), respectively. The mass loss of each NC resulted from ligand exchange and PEG modification. As such, the mass loss was divided into two regimes corresponding to ligand and PEG decomposition, respectively. The ligands and PEG molecules decompose at respective temperatures of ∼270 and 360 °C.

To evaluate the saturation magnetization at 300 K, the magnetizations of the FeNi NCs before the phase transfer were determined as a function of the external magnetic field (Figure 4). The OA-FeNi NCs exhibited excellent magnetic properties and negligible hysteresis. The maximum magnetization of OA-FeNi NCs reached 88 emu g^{-1} between the magnetization range

DOI: 10.1021/acsami.5b03952
ACS Appl. Mater. Interfaces 2015, 7, 15522−15530

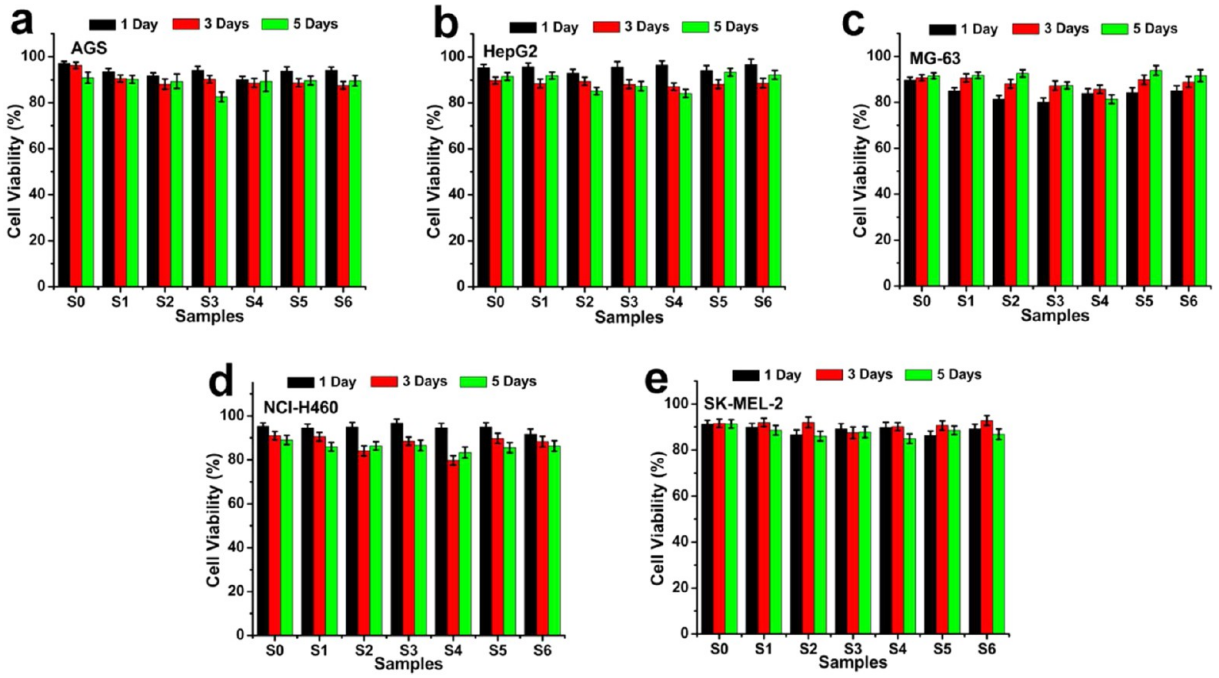

Figure 5. Relative cell viability of different cell lines [(a) AGS, (b) HepG2, (c) MG63, (d) NCI-H460, (e) SK-MEL-2] exposed to two different concentrations of modified FeNi NCs for 5 d (S0, control; S1, Cys-FeNi, 25 μg mL^{-1}; S2, Cys-FeNi, 50 μg mL^{-1}; S3, 5AA-FeNi, 25 μg mL^{-1}; S4, 5AA-FeNi, 50 μg mL^{-1}; S5, GSH-FeNi, 25 μg mL^{-1}; S6, GSH-FeNi, 50 μg mL^{-1}).

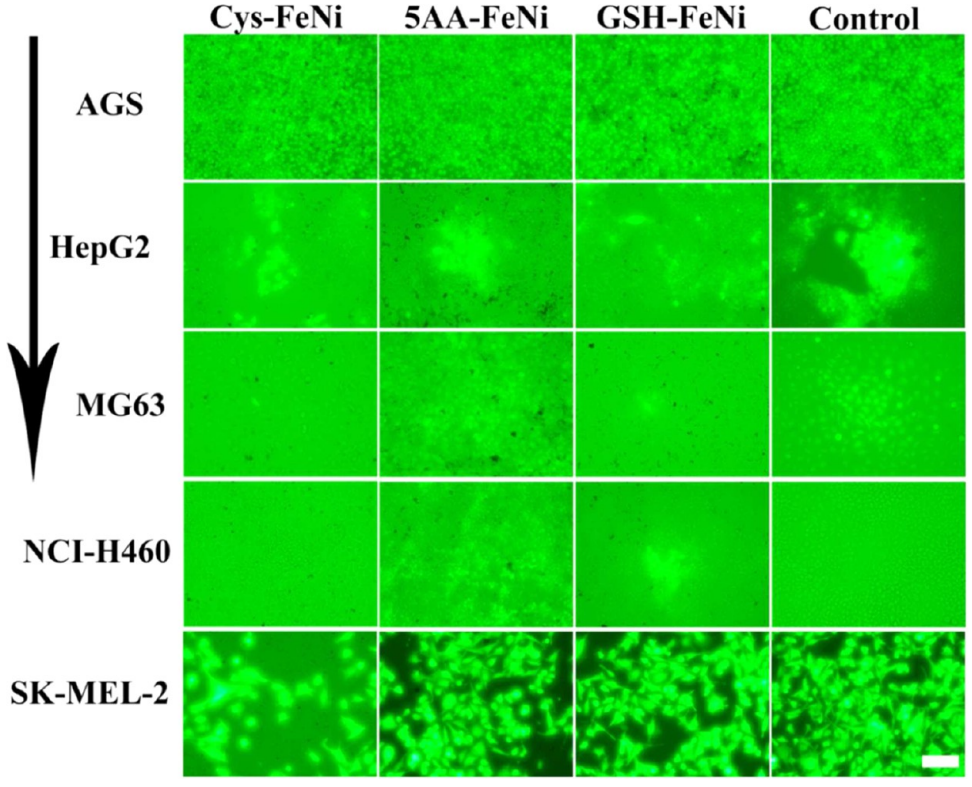

Figure 6. Representative fluorescence microscopy images of AGS, HepG2, MG63, NCI-H460, and SK-MEL-2 cells, which were treated by using 50 μg/mL colloidal solutions (Cys-FeNi, 5AA-FeNi, and GSH-FeNi NCs) after 5 days, in preparation for biocompatibility measurements. The scale bar in the inset corresponds to 20 μm.

from −3 to +3 T at 300 K (Figure 4a), and their ferromagnetic behavior resulted in relatively coercivity ∼0.015 T (5 K) and ∼0.037 T (300 K) in Supporting Information Figure S7. As expected, the modified NCs exhibit excellent magnetic properties at room temperature (300 K), in which each value of the maximum magnetization was 80.7, 79.8, 80.4 emu g^{-1} for Cys-, 5AA-, and GSH-FeNi NCs (Figure 4b−d). Notice that these values are only slightly lower than that of the OA-FeNi NCs.

DOI: 10.1021/acsami.5b03952
ACS Appl. Mater. Interfaces 2015, 7, 15522−15530

Furthermore, owing to the unaccounted weight of the capping layer,[36] iron−nickel NCs are notable in that the resulting changes from the structural component influence permeability under strong magnetic field. The exhibited H_c and μ_a cannot be reversed by electric/magnetic or degaussing processes. For instance, the measurement of magnetization at high temperature can restore the initial properties, similar to the value that was obtained after thermal annealing treatment. In addition, the electrocatalytic activity of the modified NCs (Cys-, 5AA-, and GSH-FeNi NCs) during hydrogen evolution reaction (HER) was investigated in a 2 M KOH solution by using a standard three-electrode testing system. Figure 4e shows the linear sweep voltammetry (LSV) polarization curves of the NCs. The figure reveals overpotentials of −0.47, −0.44, and 0.15 V, which correspond to currents of 105.7, 97.8, and 209 mA for the Cys-, 5AA-, and GSH-FeNi NCs, respectively. The difference in the HER catalytic measurement stems from our use of various hydrophilic surfactants for surface modification.[37] Moreover, the hydrogen bubbles formed can be easily detached from the integrated work electrode surface, thereby resulting in increased resistance owing to a decrease in the number of available active sites on the surface of the NCs. The significantly different current and voltage of the GSH-FeNi NCs, compared to those of the other two NCs, result from the active sites and structure of the fully integrated composites. These attributes lead to increased catalytic property and decreased resistance during the catalytic reactions. Owing to its active sites, GSH-FeNi exhibits better catalytic properties than those of the other two NCs.[38] This clearly demonstrates the catalytic activity of the modified NCs during HER, where different electrocatalytic effects occur owing to a series of integrated hydrophilic materials. This resulted in increased reactivity of the sites after the surface modification and also enhanced electrocatalytic activity of the NCs.[39,40]

3.3. Biocompatibility Measurement. The biocompatibility of these bimetallic FeNi NCs was evaluated via cell viability in the form of NCs-integrated-growth with different cell lines (AGS, HepG2, MG63, NCI-H460, and SK-MEL-2) for various cultivation times and colloidal concentrations (Figure 5). The cell viability in the presence of three types of modified NCs (Cys-, 5AA-, and GSH-FeNi NCs) exhibited excellent adaptation to various cells during 5 days of cultivation time. In fact, the cell exhibited >87% viability at concentrations of up to 50 μg mL^{-1}, indicating high biocompatibility. Most of the macrophages incubated with NCs were stained green, implying that the NCs were readily phagocytosed by these five cell lines and would remain predominantly in the cytoplasma for almost 5 days. As such, the NCs can be considered nontoxic magnetic candidates owing to the nature of the chemical modification (Figure 6).[41−43] Furthermore, microscopic observation of the treated cells revealed that the morphological changes of the FeNi NC groups with varying concentrations differed only slightly from those of the control group. Moreover, microscopic observation of the modified FeNi-NC-treated cells showed that, compared with that of the control group, the colloidal stability of the respective NCs changed only slightly after the 5 days of treatment (Supporting Information Figure S8). Therefore, the modified FeNi NCs constitute nontoxic candidates for the five types of cell lines. The optical images (optical microscopy images and fluorescence microscopy images) of 3 day cultures are shown in Supporting Information Figures S9 and S10, respectively.

4. CONCLUSION

A practical and effective strategy was demonstrated for synthesizing magnetic FeNi NCs. Through surface modification using different hydrophilic molecules (Cys, 5AA, and GSH), the obtained NCs were applied as a safe highly biocompatible magnetic substitute. This demonstrates the solubility and stability in aqueous media, the net neutral surface in physiological environments, consistent magnetic properties, and catalytic property of the NCs. In the *in vitro* experiment, the FeNi NCs exhibited excellent biocompatibility and magnetic properties. Therefore, low doses of these NCs should be highly efficient in magnetohyperthermia and magnetism-induced imaging applications. The scheme described in this work constitutes an effective method for preparing new types of biocompatible material candidates, which have significant potential for use in applications such as magnetic contrast agents.

■ ASSOCIATED CONTENT

Supporting Information

Additional TEM images, STEM-EDX, XRD, FT-IR, TGA, SQUID curves, and images of fluorescence-activated cell sorting (FACS) digital microscopy data. The Supporting Information is available free of charge on the ACS Publications website at DOI: 10.1021/acsami.5b03952.

■ AUTHOR INFORMATION

Corresponding Authors

*E-mail: dyhwang@pusan.ac.kr.
*E-mail: jaebeom@pusan.ac.kr.

Notes

The authors declare no competing financial interest.

■ ACKNOWLEDGMENTS

This work was supported by Basic Science Research Program through the National Research Foundation of Korea (NRF) funded by the Ministry of Education (2013004637), and Korea-Japan International Collaboration Program through the NRF, funded by the Ministry of Science, ICT, & Future Planning (no. 2014K2A2A4001081).

■ REFERENCES

(1) Kircher, M. F.; de la Zerda, A.; Jokerst, J. V.; Zavaleta, C. L.; Kempen, P. J.; Mittra, E.; Pitter, K.; Huang, R.; Campos, C.; Habte, F.; et al. A Brain Tumor Molecular Imaging Strategy Using A New Triple-Modality MRI-Photoacoustic-Raman Nanoparticle. *Nat. Med.* **2012**, *18*, 829−834.

(2) Chen, J. S.; Hsu, H. H.; Kuo, S. W.; Huang, P. M.; Lee, J. M.; Lee, Y. C. Management of Recurrent Primary Spontaneous Pneumothorax after Thoracoscopic Surgery: Should Observation, Drainage, Redo Thoracoscopy, or Thoracotomy be Used? *Surgical Endoscopy* **2009**, *23*, 2438−2444.

(3) Mazaleyrat, F.; Varga, L. K. Ferromagnetic Nanocomposites. *J. Magn. Magn. Mater.* **2000**, *215*, 253−259.

(4) Turgut, Z.; Nuhfer, N. T.; Piehler, H. R.; McHenry, M. E. Magnetic Properties and Microstructural Observations of Oxide Coated FeCo Nanocrystals Before and After Compaction. *J. Appl. Phys.* **1999**, *85*, 4406−4408.

(5) Zhao, Y. W.; Zhang, T.; Xiao, J. Q. Explosion Compacted FeCo Particles Coated with Ferrites: A Possible Route to Achieve Artificial Soft Ferrites. *J. Appl. Phys.* **2003**, *93*, 8014−8016.

(6) Vopson, M. M. Fundamentals of Multiferroic Materials and Their Possible Applications. *Crit. Rev. Solid State Mater. Sci.* **2015**, *40*, 223−250.

DOI: 10.1021/acsami.5b03952
ACS Appl. Mater. Interfaces 2015, 7, 15522−15530

(7) Malaibari, Z. O.; Croiset, E.; Amin, A.; Epling, W. Effect of Interactions Between Ni and Mo on Catalytic Properties of A Bimetallic Ni-Mo/Al_2O_3 Propane Reforming Catalyst. *Appl. Catal., A* **2015**, *490*, 80−92.
(8) Jandl, I.; Ipser, H.; Richter, K. W. Phase Equilibria and Structural Investigations of the General NiAs-type in the Ternary System NiPtSn. *J. Alloys Compd.* **2015**, *618*, 803−814.
(9) Sharifi, E.; Salimi, A.; Shams, E.; Noorbakhsh, A.; Amini, M. K. Shape-Dependent Electron Transfer Kinetics and Catalytic Activity of NiO Nanoparticles Immobilized onto DNA Modified Electrode: Fabrication of Highly Sensitive Enzymeless Glucose Sensor. *Biosens. Bioelectron.* **2014**, *56*, 313−319.
(10) Issa, B.; Obaidat, I. M.; Albiss, B. A.; Haik, Y. Magnetic Nanoparticles: Surface Effects and Properties Related to Biomedicine Applications. *Int. J. Mol. Sci.* **2013**, *14*, 21266−21305.
(11) Petzold, J. Advantages of Soft Magnetic Nanocrystalline Materials for Modern Electronic Applications. *J. Magn. Magn. Mater.* **2002**, *242*, 84−89.
(12) Zheng, X.; Yuan, S.; Tian, Z.; Yin, S.; He, J.; Liu, K.; Liu, L. Nickel/Nickel Phosphide Core Shell Structured Nanoparticles: Synthesis, Chemical, and Magnetic Architecture. *Chem. Mater.* **2009**, *21*, 4839−4845.
(13) Li, Z.; Mo, L.; Kathiraser, Y.; Kawi, S. Yolk Satellite Shell Structured Ni@Yolk@ Ni@ SiO_2 Nanocomposite: Superb Catalyst toward Methane CO_2 Reforming Reaction. *ACS Catal.* **2014**, *4*, 1526−1536.
(14) Moghimi, N.; Bazargan, S.; Pradhan, D.; Leung, K. T. Phase-Induced Shape Evolution of FeNi Nanoalloys and Their Air Stability by In-Situ Surface Passivation. *J. Phys. Chem. C* **2013**, *117*, 4852−4858.
(15) Moghimi, N.; Abdellah, M.; Thomas, J. P.; Mohapatra, M.; Leung, K. T. Bimetallic FeNi Concave Nanocubes and Nanocages. *J. Am. Chem. Soc.* **2013**, *135*, 10958−10961.
(16) Adeyeye, A. O.; Bland, J. A. C.; Daboo, C.; Lee, J.; Ebels, U.; Ahmed, H. Size Dependence of the Magneto Resistance in Submicron FeNi Wires. *J. Appl. Phys.* **1996**, *79*, 6120−6122.
(17) Viau, G.; Fievet-Vincent, F.; Fievet, F. Nucleation and Growth of Bimetallic CoNi and FeNi Monodisperse Particles Prepared in Polyols. *Solid State Ionics* **1996**, *84*, 259−270.
(18) Das, G. K.; Stark, D. T.; Kennedy, I. M. Potential Toxicity of Up-Converting Nanoparticles Encapsulated with A Bilayer Formed by Ligand Attraction. *Langmuir* **2014**, *30*, 8167−8176.
(19) Sukthankar, P.; Avila, L. A.; Whitaker, S. K.; Iwamoto, T.; Morgenstern, A.; Apostolidis, C.; Liu, K.; Hanzlik, R. P.; Dadachova, E.; Tomich, J. M. Branched Amphiphilic Peptide Capsules: Cellular Uptake and Retention of Encapsulated Solutes. *Biochim. Biophys. Acta, Biomembr.* **2014**, *1838* (9), 2296−2305.
(20) Wang, W.; Ji, X.; Na, H. B.; Safi, M.; Smith, A.; Palui, G.; Perez, J. M.; Mattoussi, H. Design of a Multi-Dopamine-Modified Polymer Ligand Optimally Suited for Interfacing Magnetic Nanoparticles with Biological Systems. *Langmuir* **2014**, *30*, 6197−6208.
(21) Hoffmann, R.; Imamura, A.; Hehre, W. J. Benzynes, Dehydro-Conjugated Molecules, and the Interaction of Orbitals Separated by a Number of Intervening Sigma Bonds. *J. Am. Chem. Soc.* **1968**, *90*, 1499−1509.
(22) Galperin, M.; Ratner, M. A.; Nitzan, A.; Troisi, A. Nuclear Coupling and Polarization in Molecular Transport Junctions: Beyond Tunneling to Function. *Science* **2008**, *319*, 1056−1060.
(23) Wimley, W. C.; Selsted, M. E.; White, S. H. Interactions Between Human Defensins and Lipid Bilayers: Evidence for Formation of Multimeric Pores. *Protein Sci.* **1994**, *3*, 1362−1373.
(24) Mu, Q.; Jiang, G.; Chen, L.; Zhou, H.; Fourches, D.; Tropsha, A.; Yan, B. Chemical Basis of Interactions Between Engineered Nanoparticles and Biological Systems. *Chem. Rev.* **2014**, *114*, 7740−7781.
(25) Liu, Y.; Chen, T.; Wu, C.; Qiu, L.; Hu, R.; Li, J.; Cansiz, S.; Zhang, L.; Cui, C.; Zhu, G.; et al. Facile Surface Functionalization of Hydrophobic Magnetic Nanoparticles. *J. Am. Chem. Soc.* **2014**, *136*, 12552−12555.
(26) Zhang, T.; Ge, J.; Hu, Y.; Yin, Y. A General Approach for Transferring Hydrophobic Nanocrystals into Water. *Nano Lett.* **2007**, *7*, 3203−3207.
(27) Sofia, S. J.; Premnath, V.; Merrill, E. W. Poly (ethylene oxide) Grafted to Silicon Surfaces: Grafting Density and Protein Adsorption. *Macromolecules* **1998**, *31*, 5059−5070.
(28) Rao, J. P.; Gruenberg, P.; Geckeler, K. E. Magnetic Zero-Valent Metal Polymer Nanoparticles: Current trends, Scope, and Perspectives. *Prog. Polym. Sci.* **2015**, *40*, 138−147.
(29) Zhang, Y.; Hsu, B. Y. W.; Ren, C.; Li, X.; Wang, J. Silica-Based Nanocapsules: Synthesis, Structure Control and Biomedical Applications. *Chem. Soc. Rev.* **2015**, *44*, 315−335.
(30) Kuhlicke, A.; Rylke, A.; Benson, O. On-Demand Electrostatic Coupling of Individual Precharacterized Nano-and Microparticles in a Segmented Paul Trap. *Nano Lett.* **2015**, *15*, 1993−1999.
(31) Dugyala, V. R.; Daware, S. V.; Basavaraj, M. G. Shape Anisotropic Colloids: Synthesis, Packing Behavior, Evaporation Driven Assembly, and Their Application in Emulsion Stabilization. *Soft Matter* **2013**, *9*, 6711−6725.
(32) Serrano, C.; Garcia-Fernandez, L.; Fernandez-Blazquez, J. P.; Barbeck, M.; Ghanaati, S.; Unger, R.; Kirkpatrick, J.; Arzt, E.; Funk, L.; Turon, P.; et al. Nanostructured Medical Sutures with Antibacterial Properties. *Biomaterials* **2015**, *52*, 291−300.
(33) Xu, R.; Hu, B.; He, Q.; Cai, J.; Pan, Y.; Shen, J. Effect of Compound Inorganic Nano-Stabilizer on the Stability of High Concentration Coal Water Mixtures. *Fuel* **2006**, *85*, 2524−2529.
(34) Papisov, M. I.; Bogdanov, A., Jr; Schaffer, B.; Nossiff, N.; Shen, T.; Weissleder, R.; Brady, T. J. Colloidal Magnetic Resonance Contrast Agents: Effect of Particle Surface on Biodistribution. *J. Magn. Magn. Mater.* **1993**, *122*, 383−386.
(35) Sperling, R. A.; Parak, W. J. Surface Modification, Functionalization and Bioconjugation of Colloidal Inorganic Nanoparticles. *Philos. Trans. R. Soc., A* **2010**, *368*, 1333−1383.
(36) Luigjes, B.; Woudenberg, S. M.; de Groot, R.; Meeldijk, J. D.; Torres Galvis, H. M.; de Jong, K. P.; Philipse, A. P.; Erne, B. H. Diverging Geometric and Magnetic Size Distributions of Iron Oxide Nanocrystals. *J. Phys. Chem. C* **2011**, *115*, 14598−14605.
(37) Hang, T.; Hu, A.; Ling, H.; Li, M.; Mao, D. Super-Hydrophobic Nickel Films with Micro-Nano Hierarchical Structure Prepared by Electro Deposition. *Appl. Surf. Sci.* **2010**, *256*, 2400−2404.
(38) Ji, X.; Blaszczyk, J.; Xiao, B.; O'Donnell, R.; Hu, X.; Herzog, C.; Singh, S. V.; Zimniak, P. Structure and Function of Residue 104 and Water Molecules in the Xenobiotic Substrate-Binding Site in Human Glutathione S-Transferase P_{1-1}. *Biochemistry* **1999**, *38*, 10231−10238.
(39) Ding, Q.; Liu, M.; Miao, Y. E.; Huang, Y.; Liu, T. Electrospun Nickel-Decorated Carbon Nanofiber Membranes As Efficient Electrocatalysts for Hydrogen Evolution Reaction. *Electrochim. Acta* **2015**, *159*, 1−7.
(40) Ahn, S. H.; Hwang, S. J.; Yoo, S. J.; Choi, I.; Kim, H. J.; Jang, J. H.; Nam, S. W.; Lim, T. H.; Lim, T.; Kim, S. K.; et al. Electrodeposited Ni Dendrites with High Activity and Durability for Hydrogen Evolution Reaction in Alkaline Water Electrolysis. *J. Mater. Chem.* **2012**, *22*, 15153−15159.
(41) Hou, Y.; Yu, J.; Yang, W. Magnetic-Metallic Nanostructures for Biological Applications. *Metallic Nanostructures*; Springer: New York, 2015; pp 175−203.
(42) Wang, D.; Astruc, D. Fast-Growing Field of Magnetically Recyclable Nanocatalysts. *Chem. Rev.* **2014**, *114*, 6949−6985.
(43) Zhou, H.; Choi, S. I.; Zou, F.; Oh, S.; Kim, J. E.; Hwang, D. Y.; Lee, J. Cytotoxicity and Gene Expression in Sarcoma 180 Cells in Response to Spiky Magnetoplasmonic Supraparticles. *ACS Appl. Mater. Interfaces* **2014**, *6*, 19680−19689.

DOI: 10.1021/acsami.5b03952
ACS Appl. Mater. Interfaces 2015, 7, 15522−15530